Published in "Angewandte Chemie International Edition
doi: 10.1002/anie.201407728, 2014"
which should be cited to refer to this work.

Supplementary Information

Sample Preparation

Layers of *Allium cepa* cells were isolated from freshly dissected bulb scale leaves. Cells of *Allium cepa* were selected for this proof of concept experiment because the presence of the cell wall imparts rigidity to the cell and facilitates its handling. However, the measurement can in principle be performed on any kind of cell that can retain it structure through the measurement. Square samples of ca. 2 cm^2 were prepared, placed in sterile cell culture dishes and then incubated at room temperature (RT) in a 1 mM aqueous solution of the stable, water soluble tetraethyl ammonium salt of the fac-$[Re(CO)_3(Br)_3]^{2-}$. In aqueous solution the complex exchanges the Br^- ligands with water, forming Complex (1). The incubation medium consisted of ultrapure water whose pH remained constant at a value of 6.6. After 4h of incubation, cell layers were removed from solution, washed several times in fresh water while gently vortexed. The samples were then allowed to dry between two custom-designed metallic plates which housed a central opening of ca. 1 cm^2 from which the final samples were isolated. Cell layers obtained by this procedure were then carefully dissected under a microscope to yield a 1500 x 180 µm strip (see Supplementary Figure 1a) which was fixed for inspection on a polyimide 0.02 x 0.4mm Elliptical Mounted LithoLoop (Molecular Dimensions Ltd) (see Supplementary Figure 1b).

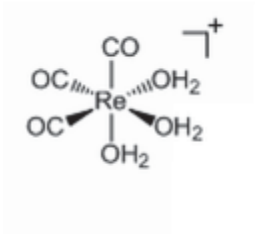

Supplementary Scheme 1. Structure of Complex 1, fac-$[Re(CO)_3(H2O)_3]^+$

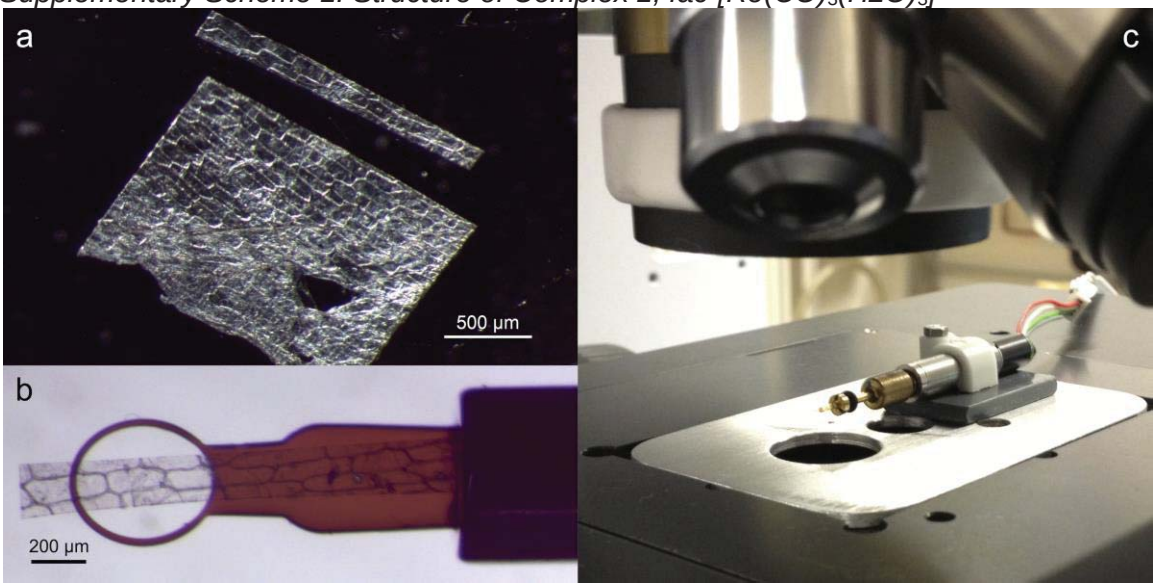

Supplementary Figure 1 a) One stripe of a single cell layer of Allium cepa was dissected

under the microscope. b) The cell stripe mounted on LithoLoop. c) Setup for rotating the sample on the sample stage of the Bruker Hyperion 3000 microscope.

FTIR Spectrometer and Microscope Setup

Infrared tomography measurements were performed on a Bruker Vertex 70v FTIR Spectrometer (Bruker Optics, Ettlingen, Germany) and a Bruker Hyperion 3000 microscope equipped with Schwarzschild optics at the department of Geosciences of Eberhard-Karls Universität Tuebingen. Images were collected by a nitrogen-cooled focal plane array (FPA) MCT imaging detector with 64 x 64 elements in transmission mode, using a 15x objective and condenser pair of Schwarzschild objectives (pixel size 2.7 x 2.7 µm in sample plane). The spectrometer was operated with a KBr-supported Ge-multilayer beamsplitter allowing coverage of the full mid-IR range. For each projection 64 scans were collected with a Forward-Backward scan at 4 cm^{-1} resolution and an interferometer scan rate of 1.6 kHz. Single channel spectra were obtained by performing a Fourier Transformation of the interferogram after apodization with a Blackman-Harris 3-Term function, using a zero-filling factor of 2 and a Power phase correction. Data were collected and saved over the 900 – 3900 cm^{-1} spectral range. A representative spectrum is presented in Supplementary Figure 2. The spectrum shows that the main bands from cellular and exogenous molecules give rise to absorption values of about 0.1 to 0.4 au. The baseline shows a tilt by about 0.2 au over 1000 cm^{-1}. This is presumably due to a combination of the absorption tail from the OH stretching band, collective modes involving H-bonded networks of OH (from the abundant polysaccharides, particularly in the cell wall and related structures) and non-absorption effects, such as refraction, reflection and scattering. Heavily distorted bandshapes, which suggest a major spectral contribution from scattering effects, are observed only on some locations of the cell wall.

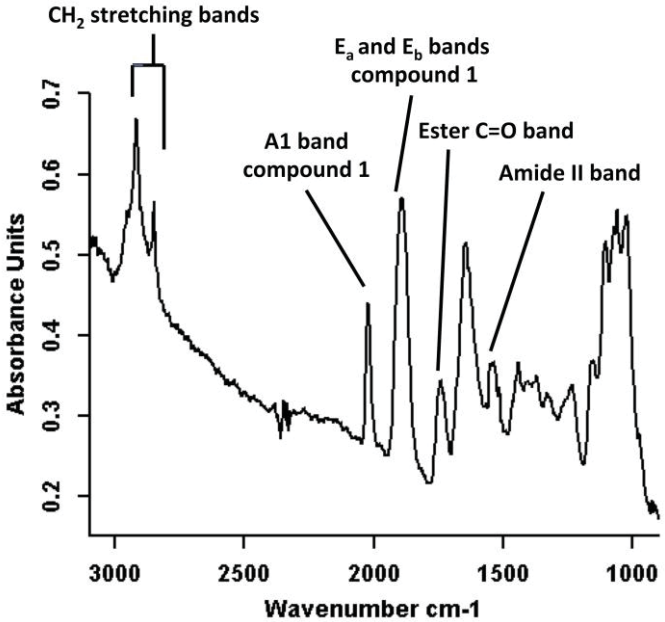

Supplementary Figure 2. Sample IR absorption spectrum from one pixel of a 2D image, approximately in the location of particle B in Figure 1. Some of the main bands used for plotting IR images are indicated.

Data acquisition

The sample was centered so that a full single cell was imaged by two adjoining frames collected by the FPA detector of the previously described setup. Effectively the measurement is the simplest case of mosaic tomography.[1] The sample was rotated around the length axis of the cell stripe which was arranged perpendicular to the beampath. The rotation was performed over ±76° in 4° steps using a stepper motor with a planetary gearhead (0620-RC-V6-05 061K1024:1, Faulhaber, Germany) and a custom-made sample holder (Supplementary Figure 1c)
For each measurement a 2D representation of composition was obtained by mapping the area or intensity of specific absorption bands over the sample projection surface. The area of complex bands and multiplets was determined by direct integration of bands above a linear baseline (Method B as defined in OPUS software). The intensity and area of specific bands that are components of complex multiplets was obtained by curve fitting Gaussian/Lorentzian bandshapes to the multiplet. For tomographic reconstruction, maps of the areas or intensities of specific bands were exported as ASCII files for import in Fiji.

Spectral Curve Fitting
Curve fitting was first performed on an individual pixel spectrum using the Levenberg-Marquardt method. A composite 50%/50% Gaussian/Lorentzian bandshape was chosen for all bands. A linear baseline was also used. Starting intensity, width, position and number of bands were chosen so as to provide a first approximation that includes all the peaks and shoulders in the experimental spectrum. Intensity, width and position of all bands, plus the factors of the linear baseline, were then all floated until convergence. This single spectrum fit was then used as the starting model to automatically fit all the spectra in the pixels of all projections. For this latter extended fit only baseline values and Lorentzian/Gaussian band intensities were allowed to float until convergence. The resulting intensity values (or the derived band areas) were used for mapping corresponding bands throughout the projections.

3D reconstruction
2D IR images were converted into MRC-format using Fiji,[2] each file representing a tilt series of 39 images from -76° to +76° in 4° steps of one specific IR absorption band. The two individual frames were stitched in Fiji using the 3D stitching plugin and a manually selected lateral offset. The resulting images were normalized by a linear histogram stretch to 8 bit image depth. The tilt series were then aligned using IMOD (V. 4.7.3).[3] The required image shifts were calculated based on cross-correlations of the average absorption images over the full IR range; these image shifts were applied to each individual dataset of a specific absorption band. The 3D reconstructions were also done using IMOD applying the SIRT algorithm with 50 iterations. The resulting volume datasets were converted into multilayered TIFF-files using Fiji. The histogram was stretched linearly and the homogeneous background absorption was removed with the lower threshold. The same settings were applied for the entire 3D dataset. For visualization both the 3D Viewer plugin (release 10.9.2012)[4] for Fiji (Figure 3) and the software package Chimera (V 1.8.1)[5] (Figures 1 & 2) were used.

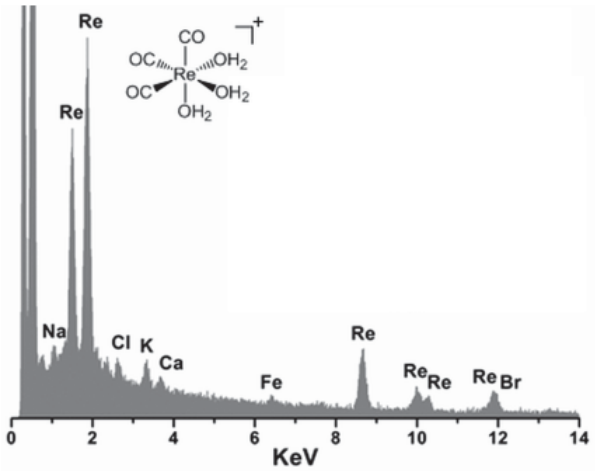

Supplementary Figure 3. Energy dispersive X-ray microanalysis (EDXMA) spectrum of the Allium cepa cell shown in this work after incubation with 1.

Absorption Coefficients

As in all applications of Beer-Lambert Law, the selection of a good absorption coefficient is critical for obtaining an accurate quantitative measurement. In many cases the availability of such coefficients will be the limiting factor in accuracy. For maximum accuracy, absorption coefficients should be determined by using standard solutions that re-create the molecular environment of the absorbing chromophore in the sample. An additional factor that requires careful attention when applying Beer-Lambert Law in a microscopy configuration is the determination of the optical path length. In a standard transmission measurement with a nearly parallel beam travelling perpendicular to sample, such as when using the sample compartment of an interferometer, the sample thickness is used as the optical path length as the two practically coincide. This is not the case when performing a microscopy measurement. The rays propagating from an objective cross the sample at different angles. In the case of a Schwarzschild objective, common in IR microscopy applications, no rays are perpendicular to the sample, because of the cone of shadow generated by the secondary mirror. It follows that the optical path length through a flat sample perpendicular to the microscope axis is longer than the sample thickness. The difference can be estimated to be about 8% and 15% of sample thickness for the 15x and 36x objectives used in a Bruker Hyperion 3000 microscope. Using the sample thickness as the optical path length would introduce a corresponding systematic error into the measurement. An additional complication in determining the optical path length is given by the fact that at the focal point diffraction effects create a complex distribution of light intensity. Finally, if the distribution of light through the pupil of the objective is not uniform and not stable over time, such as when using a synchrotron source, it becomes nearly impossible to accurately know the optical path length from experiment to experiment. A practical way to address all these issues without compromising accuracy is to determine the absorption coefficients by measuring a standard solution, of the same or similar thickness as that of the sample, with the same objective and alignment used for the final measurement. In this way all the geometrical parameters that affect the optical path length are the same in the measurement of the standard and of the sample.

The absorption coefficient for band A1 of compound 1, $\varepsilon = 6.67*10^{-4}\ \mu m^{-1}\ mM^{-1}$, was

determined by measuring the absorbance of a 10 μm thick aqueous solution of 1 of known concentration with the same microscope and objectives used for the tomography experiment. The absorption coefficient of the CO ligands of Re complexes is expected to vary according to the nature of the other ligands in the first coordination sphere. In the nuclear environment, water molecules, hydroxyl groups from the nucleic acid backbone or DNA bases are likely ligands for the metal center. These would have similar effect on the absorption coefficient of the CO ligands, thus justifying the use of an absorption coefficient determined in aqueous solution.

Other molecules can be quantified in a similar way provided that an appropriate absorption coefficient can be obtained. In many cases this may not be feasible, thus preventing or limiting the accurate measurement of some molecular concentrations. In these cases the concentration of other molecules can still be estimated, although with lower accuracy, by using average absorption coefficients or absorption coefficients obtained from related compounds (e.g. $3.5*10^{-5}$ mM^{-1} μm^{-1} for the peptide bond absorption around 1650 cm^{-1})

Calculation of Absorption from the Nucleus

Measuring the absorption of a specific portion of the image requires a correction for the absorption of other portions of the sample that are crossed by the beam and thus contribute to total absorbance. In the specific case discussed in this work, involving the absorption of Complex 1 located in the nucleus, the contribution from absorption of Complex 1 located in the cell wall must be removed. The correction is calculated using the 3D images used the 3D reconstructions. The average intensities in the Region of Interest (ROI), in this case the nucleus, are summed up for the individual layers of voxels. This is done for the entire column with 14 slices and for the slices wherein a clear signal of the round-shaped nucleus is obviously visible. The ratio of the sums of the average intensities of these two quantities is equal to the ratio of the absorbance coming from the nucleus and from the thickness of the reconstructed volume above and below it. This gives a value of 0.7 for the absorption of band A1 in the nucleus relative to the total absorption of A1 through the thickness of the sample. This value is used to extract the absorbance of the nucleus for use in Beer-Lambert law. The procedure is general and can be applied to obtain a corrected absorbance for any specific cellular structure.

Theoretical Evaluation of the Spatial Resolution

Similar to electron tomography, in IR tomography the quality of a 3D reconstruction is influenced by several experimental factors such as the total tilt range, the number of acquired 2D projection images (i.e. the angle step size during acquisition) and the alignment rotation stacks[6]. Mezerji and coworkers (2011) provide an overview of the conventional way of estimating spatial resolution. In brief, in electron tomography, Crowther et al. (1970) introduced a measure to estimate the resolution in all three dimensions of a single tilt axis geometry.[7] Assuming an ideal tilt range of ±90° and a perfect alignment of the rotation image sequence, the resolution along the tilt axis is solely limited by the resolution of the acquired 2D images. The resolution orthogonal to both the rotation and the beam axis is approximated by the following equation:

$$d=\pi*D/n \qquad (1)$$

where d is the resolution, D is the diameter of the reconstructed volume and n is the number of acquired projections.

The resolution in the direction of the beam axis is degraded by the so-called missing wedge (caused by the missing angle between the acquired angle range and ±90°.

Radermacher and colleagues (1988) introduced an elongation factor to compensate for this effect which is calculated by the following equation:

$$e=\mathrm{sqrt}((\alpha+\sin\alpha*\cos\alpha)/(\alpha-\sin\alpha*\cos\alpha) \quad (2)$$

where α stands for the maximum tilt angle.[8]

In our case, this ideal geometry is not met as our reconstructed volume is not cylindrical, but about 180μm in width, (orthogonal to both tilt rotation axis), and 54 μm in thickness, (along the beam axis). However, we use the concept to estimate boundary conditions of a worst case and an ideal case to get an approximation of the resolution of our approach. The sample geometry allowed for a total tilt range of ±76° against the plane orthogonal to the IR beam axis of the microscope. We acquired datasets in 4° steps resulting in 39 2D projections.
This results in the following approximations.
Parallel to the tilt axis, the resolution d allowed by the range of tilt angles is better than the resolution allowed by diffraction, as defined by Rayleigh's criterion ($d=0.61\lambda/NA$, where NA is the numerical aperture of the microscope objectives), for most wavelengths. The numerical aperture of the objectives (NA = 0.4) dictates that resolution in the plane perpendicular to the optical axis is limited to the range 15 μm (at 1000 cm^{-1}) to 3.8 μm (at 4000 cm^{-1}). According to equation 1, the upper and lower resolution limits, imposed by the range of tilt angles, orthogonal to both tilt and beam axis are:
upper limit: 14.5 μm
lower limit: 4.34 μm

Therefore, in the plane perpendicular to the beam axis, according to equation 2, the upper and lower resolution limits parallel to beam axis are:
upper limit: 17.3 μm
lower limit: 5.20 μm

In the direction of the beam, Rayleigh's criterion is given by $d = 2\lambda\eta/(NA)^2$, where η is the refractive index of the medium. We approximate η with 1.5, a common value for organic material, and have a diffraction limited resolution range of 188 μm (at 1000 cm^{-1}) to 47 μm (at 4000 cm^{-1}). For samples that are very large in the direction orthogonal to the rotation axis it should be considered that at high tilt angles the sample might not entirely fit into the depth of field that is several tens of μm. This could potentially affect the resolution parallel to the beam axis.
It is to be noted that the pixel size of the FPA detector, as projected in the sample plane by the 15x objectives, is 2.7 μm. Therefore, when imaging at the shorter wavelengths of the mid-IR range, around 4000 cm^{-1}, the pixel size that limits the achievable sampling frequency of the image becomes larger than the value requested by Nyquist theorem for capturing the full spatial resolution that can be achieved by optics with the resulting image resolution.

Estimation of Spatial Resolution
To assess the quality of the 3D reconstruction we evaluate the capability to resolve nucleus and spheroid in the image at 1538 cm^{-1} (λ= 6.5 μm) of Figure 2a. Supplementary Figure 4 shows the intensity profile of the pixels along the axis connecting nucleus and spherosome. Panel B plots the grayscale values along the axis, showing a saddle point with intensity about 65% of the maximum. The images of two points of equal intensity are just resolved according to Rayleigh's criterion if the saddle point is at 73.5% of the maximum. The points defining the edge of the nucleus and spherosome along the axis plotted in Supplementary Figure 4A are therefore fully

resolved according to Rayleigh's criterion.

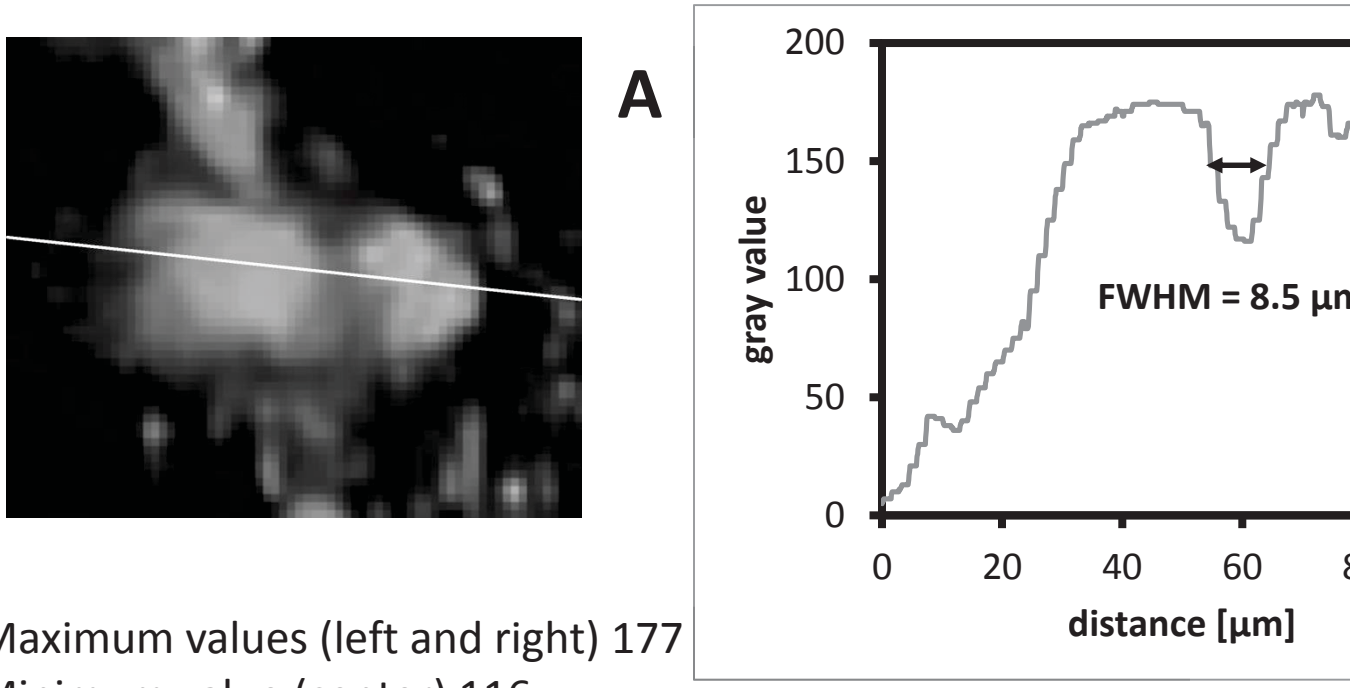

Supplementary Figure 4. Intensity profile of the grayscale values along the axis connecting nucleus and spherosome in Figure 2a. *A, Marking of the section used for the intensity profile, from the 3D image collected at 1538 cm^{-1} of Figure 2a. B, Intensity profile of the grayscale pattern from panel A.*

As discussed in the previous section, the experimental parameters chosen for the tomography retain the resolution provided by the optical system for 2D images, without additional degradation. Although we did not perform accurate measurements of resolution, the possibility to optically resolve the nucleus and spheroid with light of about 1538 cm^{-1} (6.5 µm) confirms that the resolution is 8.5 µm or better at this wavelength. Part of this is credited to the use of reflective objectives, which are free from chromatic aberrations and easily corrected for coma, astigmatism and spherical aberration.

Laser scanning microscopy

To obtain information on the structure of the analyzed *Allium cepa* cell (see Figure 3, lower row), the sample was additionally imaged in a laser scanning microscope in transmission mode (Leica SPE, 488nm laser, objective lens HCX PL Fluotar 63x, NA=0.7).

References

1 Mokso, R. *et al.* X-ray mosaic nanotomography of large microorganisms. *J Struct Biol* **177**, 233-238, doi:10.1016/j.jsb.2011.12.014 (2012).

2 Schindelin, J. *et al.* Fiji: an open-source platform for biological-image analysis. *Nat Methods* **9**, 676-682, doi:10.1038/Nmeth.2019 (2012).

3 Kremer, J. R., Mastronarde, D. N. & McIntosh, J. R. Computer visualization of three-dimensional image data using IMOD. *J Struct Biol* **116**, 71-76, doi:10.1006/Jsbi.1996.0013 (1996).

4 Schmid, B., Schindelin, J., Cardona, A., Longair, M. & Heisenberg, M. A high-level 3D visualization API for Java and ImageJ. *Bmc Bioinformatics* **11**, doi:10.1186/1471-2105-11-274 (2010).

5 Pettersen, E. F. *et al.* UCSF chimera - A visualization system for exploratory research and analysis. *J Comput Chem* **25**, 1605-1612, doi:10.1002/Jcc.20084 (2004).

6 Heidari Mezerji, H., Van den Broek, W. & Bals, S. A practical method to determine the effective resolution in incoherent experimental electron tomography. *Ultramicroscopy* **111**, 330-336, doi:10.1016/J.Ultramic.2011.01.021 (2011).

7 Crowther, R. A., Derosier, D. J. & Klug, A. Reconstruction of 3 Dimensional Structure from Projections and Its Application to Electron Microscopy. *Proc R Soc Lon Ser-A* **317**, 319-&, doi:10.1098/Rspa.1970.0119 (1970).

8 Radermacher, M. 3-Dimensional Reconstruction of Single Particles from Random and Nonrandom Tilt Series. *J Electron Micr Tech* **9**, 359-394, doi:10.1002/Jemt.1060090405 (1988).